BBA - Molecular Cell Research 1866 (2019) 1171–1179

Contents lists available at ScienceDirect

BBA - Molecular Cell Research

journal homepage: www.elsevier.com/locate/bbamcr

Applications of FLIKA, a Python-based image processing and analysis platform, for studying local events of cellular calcium signaling☆

Kyle L. Ellefsen[a], Jeffrey T. Lock[a,*], Brett Settle[a], Carley A. Karsten[a], Ian Parker[a,b]

[a] Department of Neurobiology & Behavior, UC Irvine, Irvine, CA, USA
[b] Department of Physiology & Biophysics, UC Irvine, Irvine, CA, USA

ARTICLE INFO

Keywords:
Image analysis
Ca^{2+} puffs
IP_3 receptors
Ca^{2+} signaling

ABSTRACT

The patterning of cytosolic Ca^{2+} signals underlies their ubiquitous ability to specifically regulate numerous cellular processes. Advances in fluorescence microscopy have made it possible to image these signals with unprecedented temporal and spatial resolution. However, this is a double-edged sword, as the resulting enormous data sets necessitate development of software to automate image processing and analysis. Here, we describe Flika, an open source, graphical user interface program written in the Python environment that contains a suite of built-in image processing tools to enable intuitive visualization of image data and analysis. We illustrate the utility and power of Flika by three applications for studying cellular Ca^{2+} signaling: a script for measuring single-cell global Ca^{2+} signals; a plugin for the detection, localization and analysis of subcellular Ca^{2+} puffs; and a script that implements a novel approach for fluctuation analysis of transient, local Ca^{2+} fluorescence signals. This article is part of a Special Issue entitled: ECS Meeting edited by Claus Heizmann, Joachim Krebs and Jacques Haiech.

1. Introduction

Cytosolic Ca^{2+} signals are utilized by all cells of the body to regulate cellular processes as diverse as gene transcription, secretion, mitochondrial energetics, electrical excitability and fertilization; indeed, often more than one process in the same cell [1,2]. The versatility and specificity of ubiquitous cellular Ca^{2+} signals derives from their localization in both space and time — a consequence of the rapid release of Ca^{2+} ions into the cytosol through channels in the plasma and endoplasmic reticulum (ER) membranes together with the restricted diffusion of Ca^{2+} by stationary cytosolic buffers [3]. Following the development of highly sensitive fluorescent indicator dyes [4,5] it became possible to image subcellular Ca^{2+} signals with high spatial and temporal resolution, leading to the initial discovery of local Ca^{2+} puffs originating through inositol trisphosphate receptors (IP_3Rs) in the ER membrane [6–8], followed by numerous reports of other local Ca^{2+} signals in diverse cell types, notably including sparks arising from ryanodine receptors in muscle [9,10].

Progressive technological advances in total internal reflection fluorescence (TIRF) microscopy and improved capabilities of electron-multiplied CCD (EMCCD) and scientific CMOS (sCMOS) cameras have enabled high-resolution imaging of Ca^{2+} signals in two spatial dimensions [11,12]. The evanescent field created by TIRF microscopy is used to excite the fluorescence of cytosolic Ca^{2+} indicators within a region limited to ~100 nm deep adjacent to the cell membrane, providing an optical 'section' appreciably narrower than is possible by confocal microscopy. Moreover, this sheet is continuously illuminated, as opposed to the sequential scanning of a confocal spot, so that large areas of a cell can be simultaneously imaged by a camera. Currently available cameras enable imaging with 128×128 or higher pixel spatial resolution at rates of > 1000 frames s^{-1}. This approach yields vastly more information (ca. 1 GB or more per minute) than previous techniques such as linescan imaging [13].

In the face of such large data sets, manual analysis is cumbersome, time consuming, and potentially biased and error prone. As a consequence, the need for automated image analysis algorithms that generate quantitative information has grown in recent years. This has resulted in the proliferation of algorithms and software designed for

Abbreviations: TIRF, total internal reflection fluorescence; EMCCD, electron-multiplied CCD; sCMOS, scientific complementary metal oxide semiconductor; ROI, region of interest; Ca^{2+}, calcium; ER, endoplasmic reticulum; IP_3, inositol trisphosphate; IP_3Rs, inositol trisphosphate receptors; GUI, graphical user interface; WT, wild type; KO, knock-out

☆ This article is part of a Special Issue entitled: ECS Meeting edited by Claus Heizmann, Joachim Krebs and Jacques Haiech.

* Corresponding author at: Department of Neurobiology & Behavior, University of California, Irvine, CA 92697, USA.
E-mail address: lockj@uci.edu (J.T. Lock).

https://doi.org/10.1016/j.bbamcr.2018.11.012
Received 29 August 2018; Received in revised form 20 November 2018; Accepted 22 November 2018
Available online 27 November 2018

particular uses; often so specific that their utility is limited to individual labs. Whereas many of these algorithms could be modified to solve a wide range of problems, often the steps of the algorithm remain hidden from the user, and the published details include mathematical steps that are difficult for the uninitiated to intuit. Visualization of an algorithmic step can lead to an instant and intuitive understanding of the operation, compared to difficult mathematical and verbal explanations. A picture or movie is worth a thousand equations.

There are three major programming environments currently popular for writing and sharing custom algorithms for processing and analysis of biological image data: MATLAB, ImageJ, and Python. Although MATLAB is easy to set up, it is not open source, nor is it conducive to writing large custom graphical user interface (GUI)-based programs. ImageJ is based on the Java programming language, which is not as easy for beginners as compared to Python. Python is a stable, popular programming language with many freely available open source software libraries for data and image analysis. Although many excellent libraries exist in Python, until now using them has required an intermediate level of programming experience.

Here, we describe Flika, a program that combines Python's many powerful existing image analysis libraries with a user-friendly graphical interface that requires no programming background to use. Flika contains a suite of built-in image processing tools that enable rapid, easy visualization of image data for speeding up image analysis. We illustrate the utility and power of Flika for studying cellular Ca^{2+} signaling in three applications: 1) the identification of individual cells and the processing of image stacks for measuring global (whole-cell) Ca^{2+} signals; 2) the detection, localization and analysis of subcellular (local) Ca^{2+} puffs; and, 3) a novel approach for fluctuation analysis of transient local Ca^{2+} fluorescence signals occurring during rapidly rising global Ca^{2+} levels.

2. Flika

2.1. Architecture and image import

Flika is a standalone program that runs on any platform capable of running Python (including Windows, macOS, and Linux). All of the code is open source under the MIT license and is hosted on the popular open source software sharing website GitHub (https://github.com/flika-org/flika). Once downloaded, Flika can run as a standalone program, can be launched from within a Python console (e.g. Jupyter notebook, IPython), or from within an integrated development environment (e.g. Spyder, PyCharm). When Flika is launched its main GUI is displayed, with drop-down menus bringing up options for file import/export and image processing (Fig. 1A–C). Images or image sequences (movies) can be opened: Flika supports .tif, .nd2, and .stk formats, and can easily be extended to include support for other formats. Pixel values are imported and natively stored as 64 bit floating point numbers. Thus, operations such as forming ratio images relative to baseline fluorescence that result in small, non-integer results are readily accomplished, without needing to scale up the values as required for software packages that handle only integer image data. Options are also available to change the data type of the pixel values to unsigned (uint) and signed (int) integers, ranging from 8 to 64 bits, to facilitate interactions with other software packages or to reduce computational overhead.

2.2. Image and stack processing

The image 'window' (Fig. 1D) is a central feature of Flika; operations are performed on windows to create new windows or extract data from windows. The header of each window displays both the title of the original source file, and a cumulative list of functions that have subsequently been applied. To the right of each window a histogram shows pixel intensities together with a lookup table that can be used to adjust brightness and contrast, and to apply color maps. For movies, the bottom of the window shows a timeline that allows scrolling through a movie via the mouse or arrow keys (side-to-side arrows scroll slower, up-down arrows scroll faster). Flika has a large set of built-in operations that can be performed on windows in order to generate new windows. As open source software, additional operations continue to be added to Flika. Examples are shown in the drop-down menus in Fig. 1, illustrating functions applied to manipulate image stacks (Fig. 1A); mathematical functions applied to pixel values (Fig. 1B); and spatial and temporal filtering functions (Fig. 1C). For operations that can be run in parallel, Flika distributes the workload among multiple cores of the computer, dramatically decreasing processing time. Examples of commonly used operators include Gaussian blur, temporal Butterworth filter, ratio by baseline (to generate F/F_0 images), and binary threshold.

Each operation generates a new window that can be further operated on in turn. These operations are typically performed in a sequence that will yield a processed image from which data can be readily extracted. For example, if a researcher is trying to detect signals that exist in a particular spatial-temporal frequency range, it takes mere seconds to apply a spatial filter, apply a temporal filter, apply a threshold to generate a binary image and, at the same time, visualize every intermediate step to ensure the parameters are optimized for the signal of interest. Various types of regions of interest (ROIs; square, arbitrary outline) can be drawn on windows, and can then be used, for example, to plot the average intensity of pixels inside the ROI over time (Fig. 1E). ROIs can be moved and the average intensity trace updates in real time (> 30 Hz), even for very long traces. Multiple traces from different ROIs can be overlaid, and can be analyzed from within Flika or exported for analysis in another program.

2.3. Scripting

An advantage of Flika lies in the notion that visualization of every step in a series of operations leads to a deeper and more intuitive understanding of each operation as compared to putting the chain of operations into a black box and guessing which parameters need to be changed in order to improve the output. Once a sequence of processing steps has been performed optimally, a researcher will often want to apply that same set of steps to many images of the same type. To facilitate this process, each window retains and displays in the header all the functions used to create it. These functions can be saved and run from within Flika's script editor, which includes a Python interpreter capable of executing any Python script. A script created from a window can be modified to loop over all the files in a directory and save the results.

2.4. Plugins

Although Flika's built-in functionality goes a long way towards analysis of image data, plugins extend this capability. At present, Flika has plugins for functions including particle tracking, rodent behavior analysis, myocyte counting, neuron counting, tunneling membrane nanotube detection, local and global Ca^{2+} event detection and analysis, light-sheet image analysis, and more. Flika has a built-in plugin manager that can download and install plugins stored on GitHub or other online software repositories. In this way, the Flika repository on GitHub operates analogous to an 'app store' for distributing and installing plugins written by researchers around the world.

3. Imaging methods and materials

3.1. TIRF imaging

Image data used to illustrate processing and analysis by Flika were generated by TIRF imaging utilizing a custom-built system [14], based around an Olympus IX50 microscope equipped with an Olympus 60×

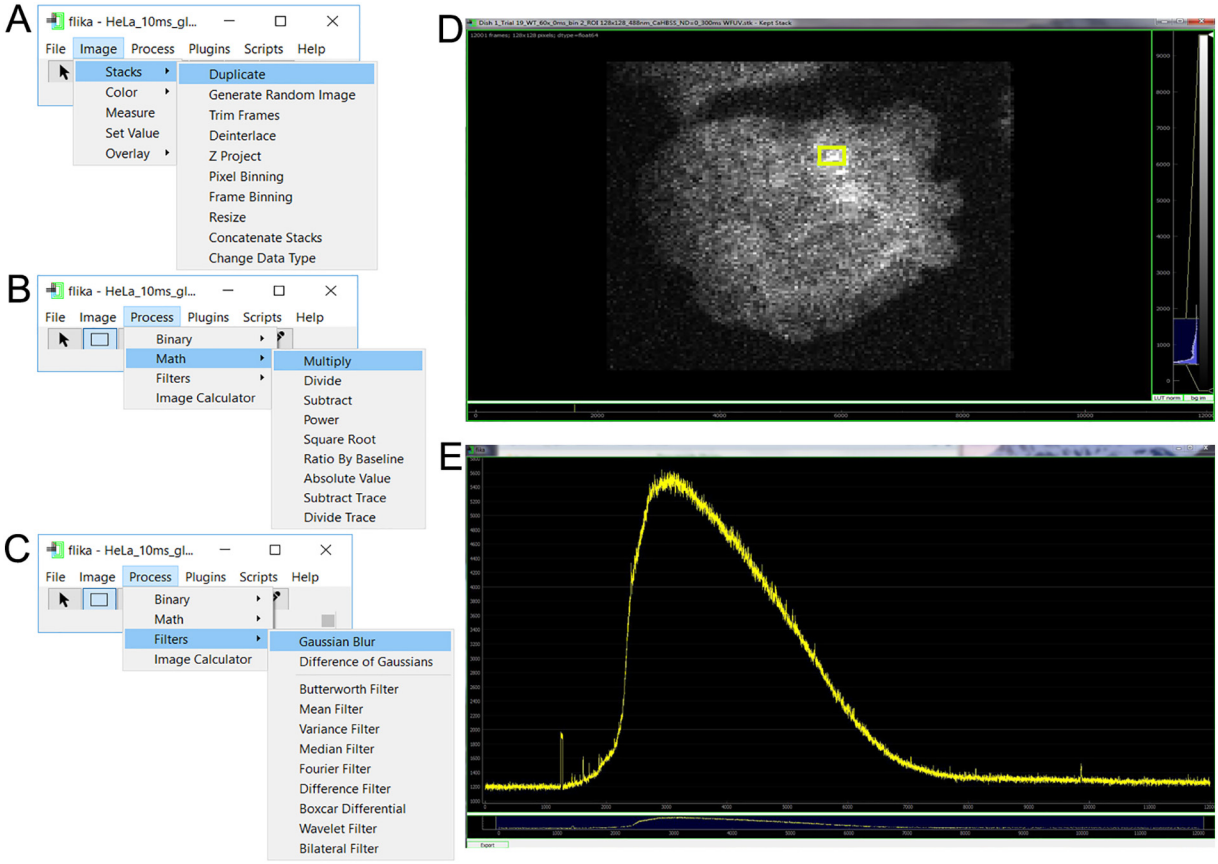

Fig. 1. Screenshots illustrating the Flika user interface. (A–C) Main Flika window, with pull-down menus showing functions for processing image stacks (A); performing pixel-level mathematical functions on images and image stacks (B); and for applying spatial and temporal filters (C). (D) Image window, displaying a selected frame of an image stack. The slider along the bottom allows scrolling through the image stack. A histogram of pixel intensity values is displayed on the right, together with sliders to adjust the range of intensities displayed and options to determine the display lookup table (monochrome or pseudocolor). (E) Window displaying a plot of intensity values averaged from the rectangular region of interest in D. The sub-window at the bottom allows the selection of the data range (frames) to be displayed in the main window, which can also be zoomed to display a range of intensity values. Moving the mouse cursor along the plot correspondingly scrolls the display in the image window. Buttons allow graphed data to be exported to a .txt file or to Excel, and to be transformed in frequency space to generate a power spectrum.

TIRF objective (NA 1.45). Fluorescence Ca^{2+} images were acquired with an Evolve EMCCD camera (Photometrics), utilizing 488 nm laser fluorescence excitation and a 510 long pass emission filter. TIRF images were captured using 2×2 pixel binning for a final field of 128×128 pixels (1 pixel = 0.53 μm) at a rate of ~125 frames s^{-1}. To photorelease i-IP_3, UV light from a xenon arc lamp was filtered through a 350–400 nm bandpass filter and introduced by a UV-reflecting dichroic in the light path to uniformly illuminate the field of view. The amount of i-IP_3 released was controlled by varying the flash duration, set by an electronically controlled shutter (UniBlitz). Image data were streamed to computer memory using Metamorph v7.7 (Universal Imaging/Molecular Devices) and stored as .stk image stack files on hard disc for offline import and analysis by Flika.

3.2. Cell culture and loading

HEK-293 cell lines were cultured in EMEM (ATCC #30-2003) supplemented with 10% FBS. Human SH-SY5Y neuroblastoma cells were cultured as described in [15]. All cell lines were maintained at 37 °C in a humidified environment composed of 95% air and 5% CO_2. Ca^{2+} imaging data illustrated in Fig. 3 were acquired from SH-SY5Y cells, loaded with Cal-520, EGTA and caged i-IP_3 as described [16]. Ca^{2+} imaging data illustrated in Fig. 2 and Figs. 5–7 were acquired from HEK-293 cells loaded as for SH-SY5Y cells with Cal-520 and caged i-IP_3, with EGTA loaded only for the experiment of Fig. 6. For imaging, cells were cultured on 35-mm glass-bottom dishes in medium containing (in mM) 135 NaCl, 5.4 KCl, 2 $CaCl_2$, 1 $MgCl_2$, 10 HEPES, and 10 glucose; pH = 7.4, at room temperature.

3.3. Materials

SH-SY5Y cells were obtained from ATCC. HEK-293 wild type cells were provided by David Yule (University of Rochester), and HEK-293 cells devoid of IP_3Rs (triple knock-out, 3KO cells) [17] were purchased from Kerafast. Membrane-permeable ester of the fluorescent Ca^{2+} dye Cal-520/AM was obtained from AAT Bioquest (#21130), of the caged IP_3 analogue ci-IP_3/PM [D-2,3,-O-Isopropylidene-6-O-(2-nitro-4,5 dimethoxy) benzyl-myo-Inositol 1,4,5,-trisphosphate Hexakis (propionoxymethyl) ester] from SiChem (cag-iso-2-145-10), and of EGTA/AM from ThermoFisher #E1219. All other reagents were from Sigma.

4. Applications

We illustrate the utility and power of Flika for processing and analyzing image stacks generated by fluorescence microscopy of cellular Ca^{2+} signals by three applications; one implemented as a plugin, and the others as scripts that utilize built-in functions of Flika.

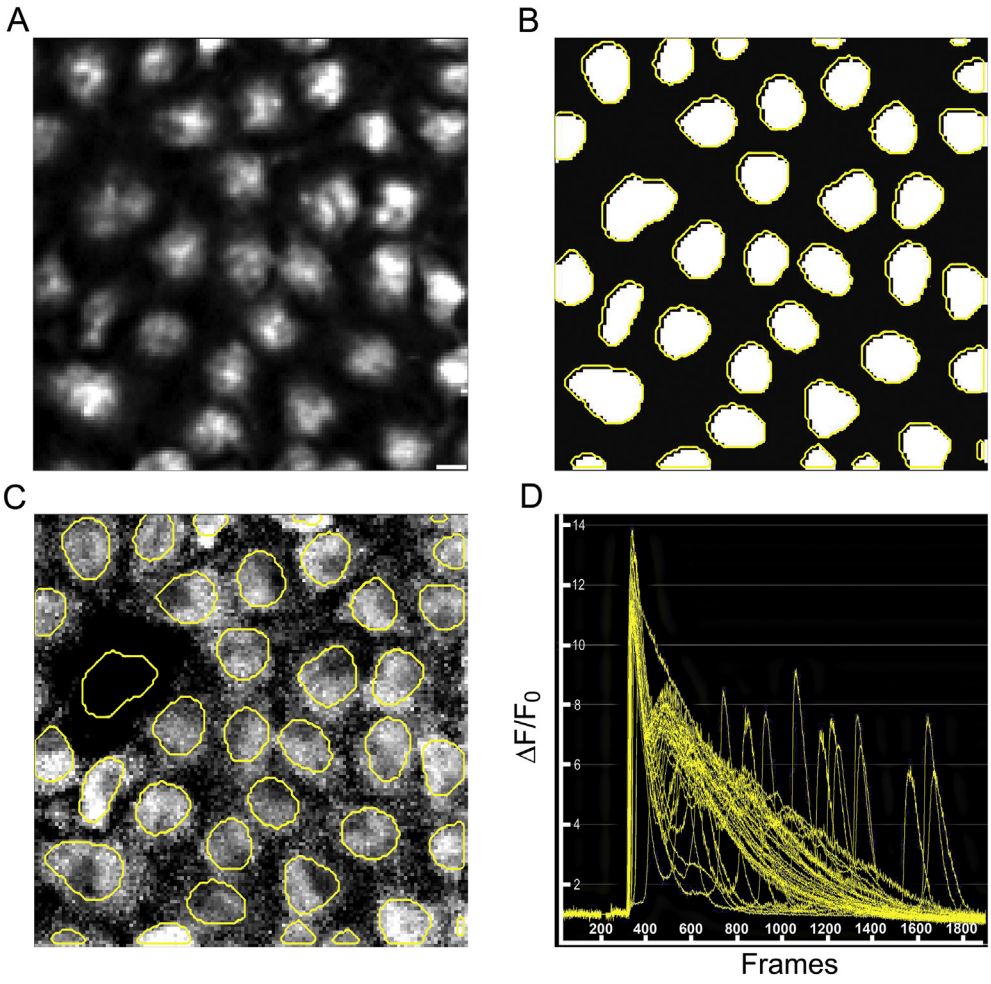

Fig. 2. Identification and analysis of global Ca^{2+} signals from multiple, individual cells. (A) The panel shows a Gaussian blurred image of resting fluorescence of Cal-520 loaded HEK-293 WT cells, averaged over ~100 frames prior to stimulation. Imaging was performed by wide-field epi-fluorescence microscopy at low (10×) magnification. Scale bar = 20 μm (B) Binarized image of A, with yellow circles illustrating the identification of individual cells performed by the 'generate ROIs' operation in Flika. (C) ROIs overlaid on a fluorescence ratio (F/F_0) image from the same image sequence as A, at a time when nearly all cells exhibited a large increase in cytosolic Ca^{2+} following stimulation by the muscarinic receptor agonist carbachol (CCH). (D) Fluorescence traces ($\Delta F/F_0$) corresponding to the average change in fluorescence over time from within each ROI shown in C (x axis labels denote frames, acquired at 100 ms intervals).

4.1. Measuring individual global Ca^{2+} signals from multiple cells

Global changes in the fluorescence intensity of cells loaded with Ca^{2+}-indicator dyes or expressing genetically encoded Ca^{2+}-indicators are commonly used as endpoint parameters of Ca^{2+} imaging experiments. The identification of cells and processing of image sequences can be easily accomplished by operations included in the drop-down menus of Flika's GUI (Fig. 1A–C) and further streamlined by the construction of short scripts that can be executed by Flika's script editor (Supplemental file 1).

Fig. 2 illustrates an example of the procedures used to measure global changes in fluorescence of Cal-520-loaded HEK-293 WT cells challenged with the muscarinic receptor agonist carbachol (CCH; 100 μM). To identify individual cells in the imaging field, a Gaussian blurred average across a user-specified number of frames in the movie ('z projection') (Fig. 2A) is first converted to a binary image from which the 'generate ROIs' operation is applied to automatically outline individual cells (Fig. 2B). Once the user-defined values are optimized for each parameter of the cell identification process, a simple script can be employed to automate the operations (Script 1; Supplemental file 1). Some final manual adjustments to the ROIs may be necessary due to incomplete separation of individual cells, after which ROIs can be saved as a .txt file and overlaid onto a movie of Ca^{2+} fluorescence ratio signals (Fig. 2C).

For single-wavelength Ca^{2+}-indicators, the background-subtracted image sequence can be converted to a fluorescence ratio ($\Delta F/F_0$) by dividing the fluorescence of every pixel (F) at each frame by the mean fluorescence of the same pixel (F_0) averaged over a specified number of initial (baseline) frames before stimulation. The beginning and end of the image sequences can be adjusted using a trim function, and artifacts, for example those arising from solution exchanges or from a flash of UV light, can be removed by setting the pixel values during these times equal to the baseline. An example of a short script that can be executed in the script editor to perform these operations is shown in Supplemental file 1 (Script 2). The average fluorescence within each ROI can be plotted over time as traces ($\Delta F/F_0$) for all cells (Fig. 2D), and the values for each ROI at every frame can be exported to an Excel file for further analysis. Measurements (e.g. peak amplitudes) can also be directly read off from plotted traces using Flika's 'measure' tool and saved for export as .txt files.

For experiments with dual wavelength Ca^{2+}-indicators such as fura-2, fluorescence ratio image sequences can be generated using the 'image calculator' function in Flika. If fluorescence from two separate excitation or emission wavelengths are alternately acquired in the same image sequence, rather than as two image files, a de-interlace operation can first be applied to separate them into two distinct image sequences before generating a fluorescence ratio.

4.2. Detecting Ca^{2+} puffs

Ca^{2+} puffs are IP_3R-mediated, localized, subcellular Ca^{2+} transients [8] that can be visualized by wide-field or TIRF microscopy of cells loaded with Ca^{2+} indicator dyes [15]. We had previously identified these events by visual inspection of image stacks (time sequences), plotting the mean intensity or fluorescence ratio change ($\Delta F/F_0$) over time as a region of interest (ROI) was moved across the cell. This detection method was labor intensive, subjective, did a poor job localizing events, and often resulted in small events being missed. To circumvent

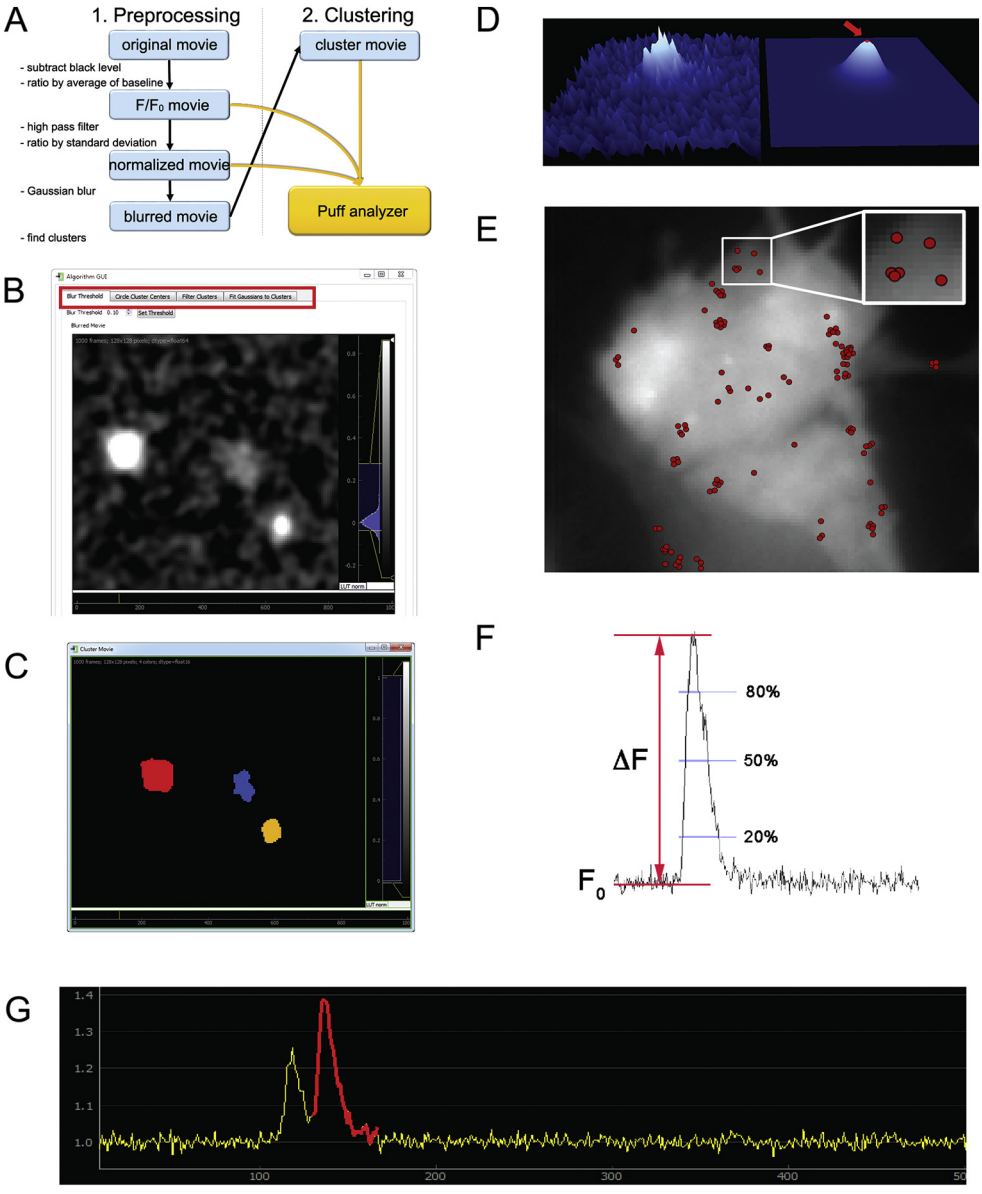

Fig. 3. Puff detect plugin. (A) Flow chart of the algorithm for image processing, event detection, localization, and analysis. (B) Example of a single frame from the fluorescence image stack after spatial and temporal filtering. (C) The same frame, after thresholding and cluster analysis to resolve and segregate discrete Ca^{2+} events, displayed in different colors. (D) Snapshot of a single puff derived from the filtered image stack and averaged over the duration of the puff, plotted with fluorescence intensity represented by color and height (left), and the two-dimensional Gaussian function fitted to this puff (right). The arrow and red dot mark the center of the Gaussian. (E) Monochrome image of the average resting fluorescence of an SH-SY5Y cell to show the cell outline, with red dots overlaid to map the centroid localizations of all observed puffs. White box shows a magnified region of the cell and accompanying puff centroid localizations. (F) The algorithm determines amplitude and kinetic parameters for each puff event as illustrated: basal resting fluorescence immediately preceding the puff, F_0; peak amplitude from baseline, ΔF; rise time from 20% to 80% of peak; fall time from 80% to 20% of peak; and full duration at half-maximal amplitude. (G) Fluorescence trace monitored from a region of interest on the original fluorescence stack. The signal from a puff whose centroid location lay within this region is colored in red.

these limitations we developed an algorithm to automate detection of puffs and serve as an unbiased detector [13]. That algorithm was originally implemented as a stand-alone application. We have now enhanced the algorithm, which runs as a plugin ('detect_puffs') that can be downloaded and run within Flika using the Plugin Manager.

Fig. 3A diagrams the processing steps within the algorithm. After importing the 'raw' fluorescence image stack, it is spatially and temporally filtered in order to minimize photon shot noise and enhance the signal-to-noise ratio of the signals of interest. The filtered movie (Fig. 3B) is then thresholded. Every pixel above a user-defined threshold is tentatively marked as being part of a Ca^{2+} release event. Then, a clustering algorithm [18] groups pixels above the threshold into puffs by identifying sites with a high density of clustered pixels relative to closely surrounding pixels and with a relatively large distance from other high-density sites. The resulting isolated puffs are depicted in different colors (Fig. 3C). At each step in the algorithm the researcher can visualize the result and adjust parameters in order to improve detection and clustering. Once the clustering of pixels into puffs is complete, a 2D Gaussian curve is fit to every event (Fig. 3D). The plugin enables interactive visualization, with representations of puffs displayed alongside their Gaussian fits (Fig. 3D) enabling visual assessment of the goodness of fit. The peak of the 2D Gaussian (red arrow) identifies with sub-pixel precision the location of the centroid of the Ca^{2+} event. Assuming the spread of the Ca^{2+} fluorescence signal is radially symmetric, this will correspond to the 'center of mass' of the ion channels underlying the event.

Once the centroids of each Ca^{2+} event are determined, they can be overlaid on an image of average fluorescence intensity to provide a map of puff sites (Fig. 3E). The criteria for grouping puff centroid localizations into puff sites is defined by the radius, in pixels, separating puff centroids from one another and is set by the user within the 'threshold-cluster' window. The grouping of puffs into discrete sites can be visualized with the 'Toggle Groups' function in the 'Puff Analyzer' window. As illustrated (Fig. 3E, inset), puffs are not randomly distributed, but rather tend to occur in tightly packed groups representing multiple events arising from a stationary cluster of IP_3Rs [19,20]. The algorithm further analyzes the temporal evolution of each puff, to determine peak amplitudes, rise times, and fall times (Fig. 3F). An ROI can be moved around the movie, updating the trace of intensity. Events colored red mark those puffs whose centroids were determined to fall inside the ROI, whereas signals arising from 'bleed-through' of fluorescence signal from more distant puff sites are colored yellow (Fig. 3G).

The user can thus visually inspect puffs, adjust start and end points of each puff, and discard events that may be artefactual. All parameters (e.g. amplitudes, kinetics, puff locations in x, y, and time) can be saved to a .txt file or to an Excel spreadsheet for further analysis, and can also be saved as a .flika file to be reloaded into the puff detect plugin at a later time.

4.3. Fluctuation analysis and visualization of local Ca^{2+} signals

The puff detect plugin (Section 3.1) is highly effective at detecting and localizing even small Ca^{2+} transients, provided they arise on a relatively stable, low level of background fluorescence. However, Ca^{2+} puffs become obscured by the much greater rise in overall fluorescence during global Ca^{2+} signals, and are thus more difficult to visualize and detect. To circumvent this limitation we developed an image processing technique of fluctuation analysis that highlights temporally rapid and spatially confined Ca^{2+} elevations, even during large amplitude global spikes. This is implemented as a script that automates a sequence of processing steps using built-in Flika functions.

4.3.1. Algorithm

Local Ca^{2+} signals such as puffs extend spatially across one or a few μm, and persist for tens or a few hundred ms. Thus, the fluorescence signals of puffs are correlated in space (across several camera pixels) and time (across several image frames). They thus represent relatively low frequency spatial and temporal signals, in contrast to 'white noise' stochastic fluctuations arising from photon shot noise that are uncorrelated across pixels and sequential frames. Our algorithm (Fig. 4A) first applies spatial and temporal filters to reduce photon shot noise and slow changes in baseline fluorescence, and then utilizes a running boxcar function to calculate, pixel-by-pixel, the variance of the fluorescence signal around the mean. Finally, remaining shot noise variance is subtracted on the basis that this is linearly proportional to the mean signal, and an image stack representing the standard deviation (SD) of fluorescence fluctuations (square root of variance) is generated for visualization.

4.3.2. Shot noise correction

The variance values not only reflect Ca^{2+}-dependent fluctuations in fluorescence of the indicator, but also the increased photon shot noise associated with increases in the mean fluorescence intensity during global responses. To correct for the latter factor, we subtract the noise variance predicted by the statistics of random shot noise. If measurements were directly in terms of numbers of detected photons, the signal variance would equal the mean. However, that was not the case for our records because of factors including the camera conversion factor (counts per photon) and the filtering applied to the image stack. We thus empirically determined an appropriate scaling factor by imaging the fluorescence emitted by a solution of fluorescein as the excitation intensity was increased (Fig. 4B). As expected, the signal variance calculated by our algorithm increased proportionally with fluorescence intensity (red trace, Fig. 4C), and a plot of variance vs. mean intensity (Fig. 4D) showed a linear relationship. We used the slope of this line to scale a copy of the original fluorescence image stack, which was then subtracted from the variance stack to yield a corrected image stack in which the mean variance was substantially independent of fluorescence intensity (blue trace, Fig. 4C).

To evaluate this method of photon shot noise correction in the context of cellular Ca^{2+} imaging, we processed records from an experiment where cytosolic [Ca^{2+}] is expected to rise in a smoothly graded manner, without overt temporal fluctuations or spatial inhomogeneities. We imaged the fluorescence of Cal-520 by TIRF microscopy in HEK-293 cells in which all IP_3 receptor isoforms were knocked out (HEK-3KO) [17], and evoked an elevation of cytosolic [Ca^{2+}] by applying a low concentration (500 nM) of ionomycin to gradually liberate Ca^{2+} sequestered in intracellular stores while eliminating influx of extracellular Ca^{2+} using a bathing solution containing no added Ca^{2+} and 300 μM EGTA. As illustrated in Fig. 5 and Video 1, this resulted in a roughly 4-fold rise in fluorescence over about 10 s, followed by a slow decline over about a minute (Fig. 5A, B, upper panels). During this response there was no appreciable increase in the mean shot noise-corrected SD (Fig. 5B, lower panel), and no spatial inhomogeneities were evident in the SD images (Fig. 5A, upper panel).

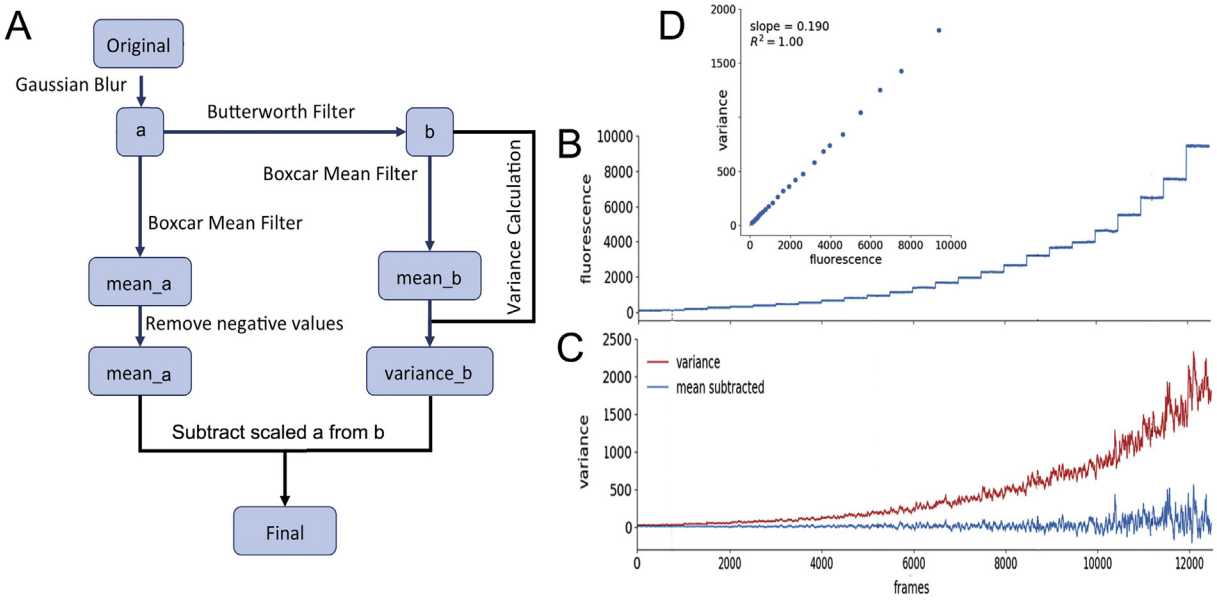

Fig. 4. Flika script for fluctuation analysis and visualization of transient, local Ca^{2+} signals. (A) Flow chart of the algorithm. Two Gaussian blurred copies are made of the original fluorescence image stack. One (a) is used to form a running mean within a time window. The other (b) is used to calculate an image stack of signal variance within the same running time window. A scaled version of image stack, a, is then subtracted from the variance stack, b, to create a final stack representing variance in excess of that predicted from photon shot noise. (B) Trace showing fluorescence measured from a small region of interest, as the laser power exciting a solution of fluorescein was increased in steps. (C) Red trace shows the corresponding increase in variance of the fluorescence from the same region. Blue trace shows variance after subtraction of predicted photon shot noise. Note that the traces in B and C show only steady state values; transitions between steps have been cropped out for clarity. (D) Plot of mean signal variance (y axis) vs. mean intensity, derived from the records in B and C.

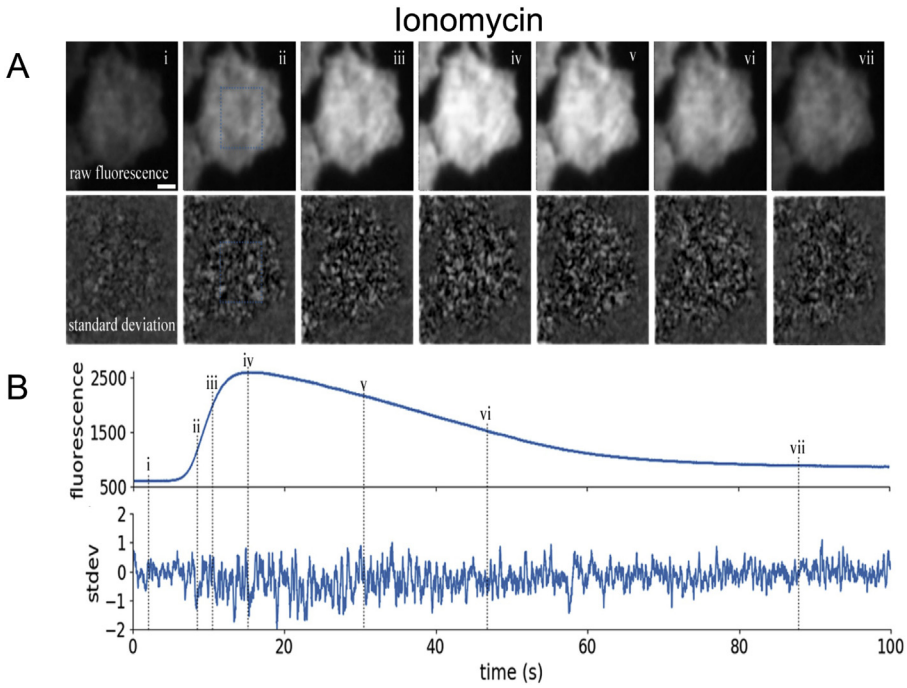

Fig. 5. Fluctuation analysis of cellular Ca^{2+} fluorescence signals in a situation where cytosolic Ca^{2+} rises homogeneously without spatial or abrupt temporal fluctuations. (A) Top panels show the 'raw' fluorescence of a HEK-3KO cell loaded with the Ca^{2+} indicator Cal-520 before (first panel) and at different times following addition of ionomycin in bath solution containing no added Ca^{2+} and 300 μM EGTA. Each panel is a single frame, acquired at an exposure time of 8 ms. The lower row of panels show shot noise-corrected SD fluctuation images at corresponding times. (B) The upper trace shows mean fluorescence (arbitrary camera units) from the region of interest marked in the second panels of A. The lower trace shows the corresponding changes in mean shot-noise corrected SD signal within the region of interest, calculated over a 30 frame (240 ms) running window. Roman numerals indicate times at which the image panels in A were obtained.

4.3.3. *Enhanced visualization of local Ca^{2+} signals*

We next evaluated the capability of fluctuation analysis to resolve local Ca^{2+} signaling events under 'easy' conditions, using weak photorelease of i-IP_3 to evoke Ca^{2+} puffs on a steady background in a cell loaded with EGTA to suppress global Ca^{2+} waves [12]. The upper panels in Fig. 6A show snapshots of Cal-520 fluorescence imaged by

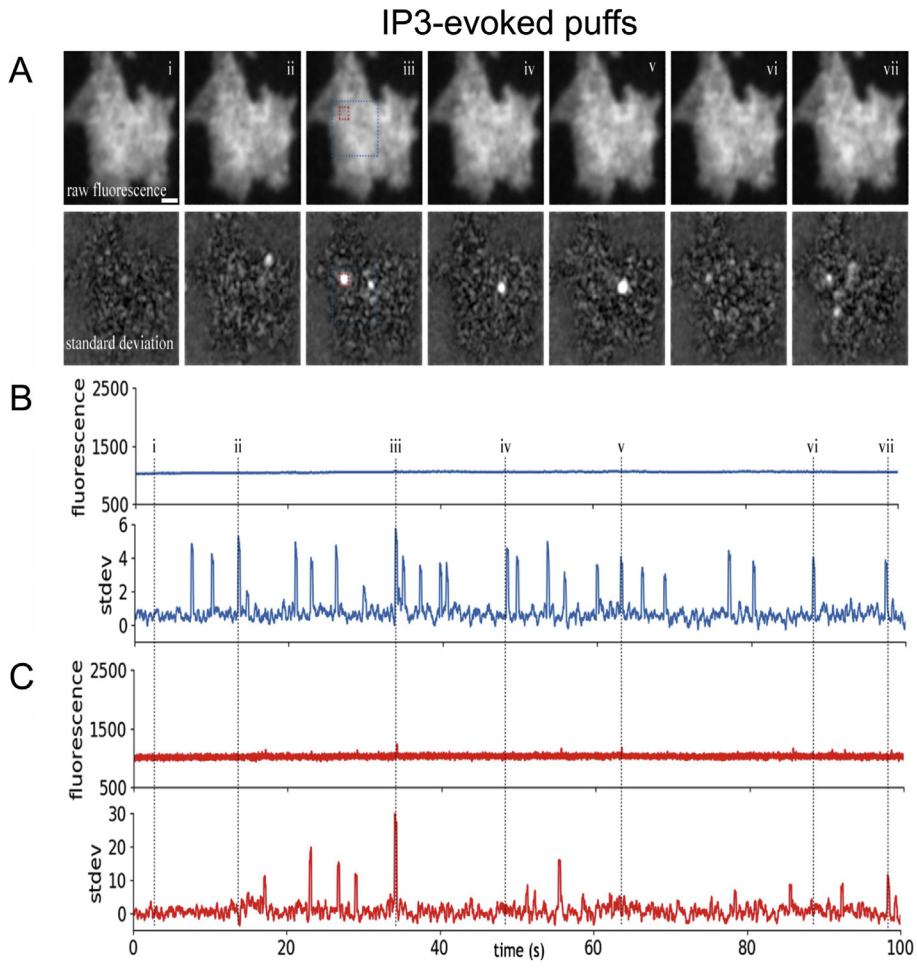

Fig. 6. Fluctuation processing enhances the visualization of local Ca^{2+} puffs. (A) Upper panels show raw fluorescence of a HEK-WT cell loaded with Cal-520, caged i-IP_3, and EGTA before (left panel) and after photorelease of i-IP_3 to evoke transient, local Ca^{2+} puffs. The lower panels show corresponding shot noise-corrected SD images. The images illustrate times when puffs were (ii, iii, iv, v vii) or were not (i, vi) evident. Roman numerals correspond to the times marked in B and C. (B) Upper trace shows mean fluorescence from the large region of interest marked in A, and the lower trace shows the corresponding mean SD signal. (C) Traces showing mean (upper) and SD (lower) signals within a small region of interest (marked in A) centered on a puff site.

TIRF microscopy in HEK-293 cells at times before and after uncaging i-IP_3. Puffs are evident in several of the panels, but are hard to discern in the raw fluorescence images. In marked contrast, corresponding SD images (lower panels, Fig. 6A) clearly highlight numerous local Ca^{2+} events arising at different sites, demonstrating the utility of this approach for enhanced visual inspection of subcellular Ca^{2+} images (Video 2). This is further illustrated by the traces in Fig. 6B, C. Measurements of fluorescence averaged across a large region of interest encompassing much of the cell showed barely detectable inflections during puffs (upper panel, Fig. 6B), whereas these signals were dramatically enhanced in the trace showing the average SD signal from the same region of interest (lower panel, Fig. 6B). Moreover, the SD trace monitored from a small region centered on a puff site (lower trace, Fig. 6C) was vastly more effective than the mean fluorescence trace (upper trace, Fig. 6C) in revealing multiple events arising at this site.

4.3.4. Fluctuation analysis of transient, local Ca^{2+} signals during global elevations of cellular Ca^{2+}

Having established that SD fluctuation images are substantially unaffected by homogeneous global Ca^{2+} elevations but highlight transient, local elevations, we then applied fluctuation analysis to look for local signals that might otherwise be obscured during cell-wide global Ca^{2+} elevations evoked by stronger photorelease of i-IP_3.

Fig. 7A and Video 3 illustrate TIRF images from HEK cells in which photorelease of i-IP_3 evoked a global elevation in Ca^{2+}, reaching a maximum fluorescence increase of about 3-times baseline, and rising and falling over a few tens of seconds. The raw fluorescence increase appeared relatively uniform across the cell throughout this response (upper panels, Fig. 7A), and the mean fluorescence averaged across a large region of interest encompassing a large fraction of the cell (blue box in second panel of Fig. 7A) showed a smooth rise and fall with barely discernable superimposed transient fluctuations (upper panel, Fig. 7B). In contrast, SD images clearly revealed an underlying flurry of localized, transient Ca^{2+} events arising at multiple sites (lower panel, Fig. 7A). Correspondingly, a trace measuring the mean SD signal from the same region of interest (lower panel, Fig. 7B) showed a large increase in fluctuations that began shortly after the UV flash, reached a maximum when the global fluorescence was rising most steeply, and persisting at a lower level for the duration of the response, even when the global fluorescence had returned almost to baseline. The traces in Fig. 7C further illustrate respective fluorescence and SD records from a small region of interest (red box in second panels of Fig. 7A) centered on a site that showed frequent, maintained local signals. Although discrete transients are only barely evident during the rising phase of the raw fluorescence trace from this site (upper panel, Fig. 7C) they are prominently displayed in the local SD trace (lower panel, Fig. 7C), although activity at individual sites is 'diluted' by averaging over a wider area in the SD trace of Fig. 7B.

4.3.5. Utility of fluctuation processing for studying local Ca^{2+} signals

We demonstrate derivation of SD image sequences by fluctuation analysis to provide a powerful aid in the visualization, detection and localization of transient, local Ca^{2+} signals. Even very low amplitude signals can be isolated from the background noise and readily visualized. However, limitations include diminished time resolution owing to the boxcar temporal windowing, so it is not possible to resolve the kinetics of individual events.

An initial conclusion from our results is that cytosolic Ca^{2+} levels during global Ca^{2+} spikes do not rise smoothly and homogeneously, as has been assumed, for example, in experiments imposing simulated Ca^{2+} oscillations ('Ca^{2+} clamp') to study gene activation [21,22]. Instead, the cell more closely resembles a bubbling cauldron of Ca^{2+}, in

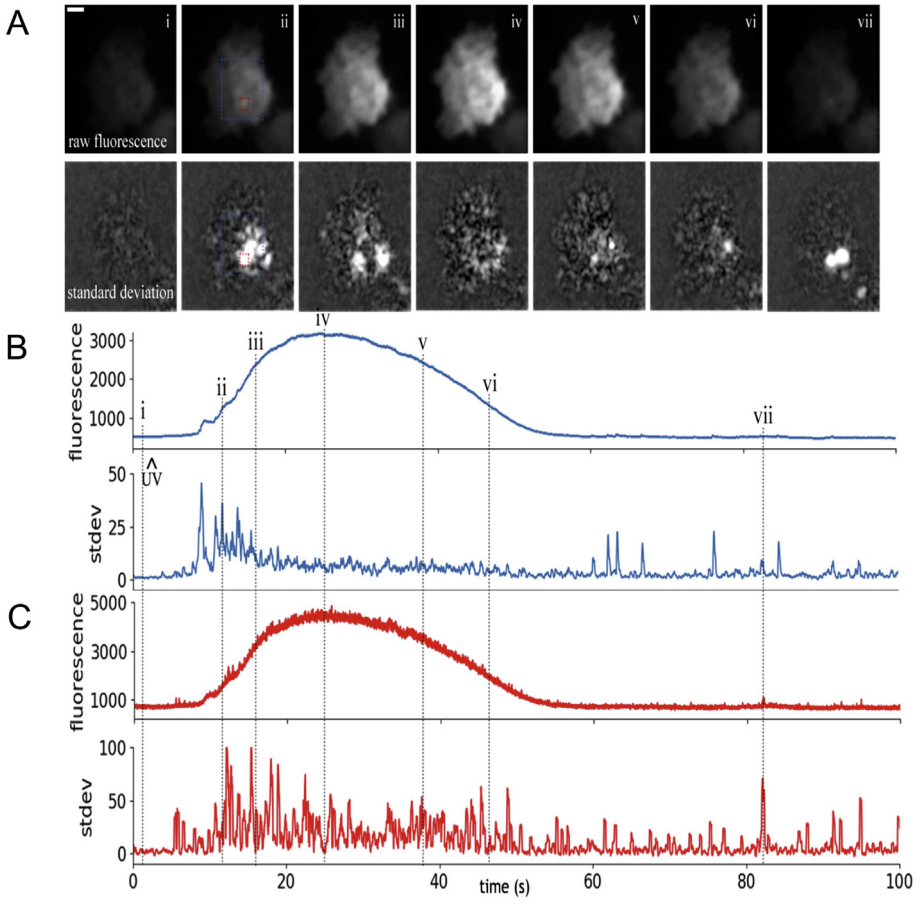

Fig. 7. Fluctuation analysis aids in detecting and locating local Ca^{2+} release events during large global elevations of cytosolic Ca^{2+}. (A) Upper panels show raw fluorescence of an HEK WT cell loaded with Cal-520 and caged i-IP_3, but without EGTA, before (left panel) and after photorelease of a greater amount of i-IP_3 to evoke a cell-wide global elevation of cytosolic Ca^{2+}. Roman numerals correspond to the times marked in B and C. The lower panels show corresponding shot-noise corrected SD images. (B) Upper trace shows mean fluorescence from the large region of interest marked in A, and the lower trace shows the corresponding mean SD signal. (D) Traces showing mean (upper) and SD (lower) signals within a small region of interest (marked in A) centered on a site of transient, local Ca^{2+} activity. (For interpretation of the references to color in this figure, the reader is referred to the web version of this article.)

which regions close to puff sites will experience abrupt, large local Ca^{2+} transients rather than a smaller, gradual elevation.

Supplementary data to this article can be found online at https://doi.org/10.1016/j.bbamcr.2018.11.012.

Transparency document.

The Transparency document associated with this article can be found, in online version.

Acknowledgements

We thank Dr. Ian Smith and Dr. Divya Swaminathan for insightful discussions concerning the imaging and detection of local Ca^{2+} signals.

Funding sources

This work was supported by the National Institutes of Health (grants R37 GM048071 and F31 GM119330).

Authors' contributions

IP directed the project and conceived the fluctuation analysis technique. KLE and BS conceived algorithms and wrote software. JTL, CAK and KLE performed experiments and analyzed data. IP, JTL and KLE wrote the manuscript. IP, KLE, JTL and CAK revised the manuscript.

Declaration of interests

The authors declare no competing interests.

References

[1] M.J. Berridge, P. Lipp, M.D. Bootman, The versatility and universality of calcium signalling, Nat. Rev. Mol. Cell Biol. 1 (2000) 11–21, https://doi.org/10.1038/35036035.
[2] D.E. Clapham, Calcium Signaling, Cell 131 (2007) 1047–1058, https://doi.org/10.1016/j.cell.2007.11.028.
[3] B. Schwaller, Cytosolic Ca(2+) buffers, Cold Spring Harb. Perspect. Biol. 2 (2010) a004051, https://doi.org/10.1101/cshperspect.a004051.
[4] G. Grynkiewicz, M. Poenie, R.Y. Tsien, A new generation of Ca^{2+} indicators with greatly improved fluorescence properties, J. Biol. Chem. 260 (1985) 3440–3450 http://www.jbc.org/content/260/6/3440.abstract.
[5] A. Minta, J.P. Kao, R.Y. Tsien, Fluorescent indicators for cytosolic calcium based on rhodamine and fluorescein chromophores, J. Biol. Chem. 264 (1989) 8171–8178 http://www.jbc.org/content/264/14/8171.abstract.
[6] Y. Yao, J. Choi, I. Parker, Quantal puffs of intracellular Ca^{2+} evoked by inositol trisphosphate in *Xenopus* oocytes, J. Physiol. 482 (1995) 533–553, https://doi.org/10.1113/jphysiol.1995.sp020538.
[7] I. Parker, Y. Yao, Regenerative release of calcium from functionally discrete subcellular stores by inositol trisphosphate, Proc. R. Soc. Lond. Ser. B Biol. Sci. 246 (1991) 269 LP–274.
[8] I. Parker, J. Choi, Y. Yao, Elementary events of InsP3-induced Ca^{2+} liberation in *Xenopus* oocytes: hot spots, puffs and blips, Cell Calcium 20 (1996) 105–121, https://doi.org/10.1016/S0143-4160(96)90100-1.
[9] H. Cheng, W.J. Lederer, M.B. Cannell, Calcium sparks: elementary events underlying excitation-contraction coupling in heart muscle, Science (80-.). 262 (1993) 740 LP-744. http://science.sciencemag.org/content/262/5134/740.abstract.
[10] H. Cheng, W.J. Lederer, Calcium sparks, Physiol. Rev. 88 (2008) 1491–1545, https://doi.org/10.1152/physrev.00030.2007.
[11] A. Demuro, I. Parker, Imaging the activity and localization of single voltage-gated Ca(2+) channels by total internal reflection fluorescence microscopy, Biophys. J. 86 (2004) 3250–3259 http://www.ncbi.nlm.nih.gov/pmc/articles/PMC1304190/.
[12] I.F. Smith, S.M. Wiltgen, I. Parker, Localization of puff sites adjacent to the plasma membrane: functional and spatial characterization of Ca^{2+} signaling in SH-SY5Y cells utilizing membrane-permeant caged IP3, Cell Calcium 45 (2009) 65–76, https://doi.org/10.1016/j.ceca.2008.06.001.
[13] K.L. Ellefsen, B. Settle, I. Parker, I.F. Smith, An algorithm for automated detection, localization and measurement of local calcium signals from camera-based imaging, Cell Calcium 56 (2014) 147–156, https://doi.org/10.1016/j.ceca.2014.06.003.
[14] A. Demuro, I. Parker, Optical patch-clamping: single-channel recording by imaging Ca^{2+} flux through individual muscle acetylcholine receptor channels, J. Gen. Physiol. 126 (2005) 179 LP–192 http://jgp.rupress.org/content/126/3/179.abstract.
[15] J.T. Lock, I. Parker, I.F. Smith, A comparison of fluorescent Ca^{2+}indicators for imaging local Ca^{2+}signals in cultured cells, Cell Calcium 58 (2015), https://doi.org/10.1016/j.ceca.2015.10.003.
[16] J.T. Lock, I.F. Smith, I. Parker, Comparison of Ca^{2+}puffs evoked by extracellular agonists and photoreleased IP3, Cell Calcium 63 (2017), https://doi.org/10.1016/j.ceca.2016.11.006.
[17] K.J. Alzayady, L. Wang, R. Chandrasekhar, L.E. Wagner, F. Van Petegem, D.I. Yule, Defining the stoichiometry of inositol 1,4,5-trisphosphate binding required to initiate Ca^{2+} release, Sci. Signal. 9 (2016) ra35 LP-ra35 http://stke.sciencemag.org/content/9/422/ra35.abstract.
[18] A. Rodriguez, A. Laio, Clustering by fast search and find of density peaks, Science (80-.). 344 (2014) 1492 LP-1496. http://science.sciencemag.org/content/344/6191/1492.abstract.
[19] I.F. Smith, S.M. Wiltgen, J. Shuai, I. Parker, Ca^{2+} puffs originate from preestablished stable clusters of inositol trisphosphate receptors, Sci. Signal. 2 (2009) ra77 LP-ra77.
[20] N.B. Thillaiappan, A.P. Chavda, S.C. Tovey, D.L. Prole, C.W. Taylor, Ca^{2+} signals initiate at immobile IP3 receptors adjacent to ER-plasma membrane junctions, Nat. Commun. 8 (2017) 1505, , https://doi.org/10.1038/s41467-017-01644-8.
[21] R.E. Dolmetsch, K. Xu, R.S. Lewis, Calcium oscillations increase the efficiency and specificity of gene expression, Nature 392 (1998) 933, https://doi.org/10.1038/31960.
[22] E. Smedler, P. Uhlén, Frequency decoding of calcium oscillations, Biochim. Biophys. Acta Gen. Subj. 1840 (2014) 964–969, https://doi.org/10.1016/j.bbagen.2013.11.015.